Review Article

Johannes Finger*, Benedikt Bornschlegel, Martin Reininghaus, Andreas Dohrn, Markus Nießen, Arnold Gillner and Reinhart Poprawe

Heat input and accumulation for ultrashort pulse processing with high average power

https://doi.org/10.1515/aot-2018-0008
Received January 25, 2018; accepted April 12, 2018; previously published online May 1, 2018

Abstract: Materials processing using ultrashort pulsed laser radiation with pulse durations <10 ps is known to enable very precise processing with negligible thermal load. However, even for the application of picosecond and femtosecond laser radiation, not the full amount of the absorbed energy is converted into ablation products and a distinct fraction of the absorbed energy remains as residual heat in the processed workpiece. For low average power and power densities, this heat is usually not relevant for the processing results and dissipates into the workpiece. In contrast, when higher average powers and repetition rates are applied to increase the throughput and upscale ultrashort pulse processing, this heat input becomes relevant and significantly affects the achieved processing results. In this paper, we outline the relevance of heat input for ultrashort pulse processing, starting with the heat input of a single ultrashort laser pulse. Heat accumulation during ultrashort pulse processing with high repetition rate is discussed as well as heat accumulation for materials processing using pulse bursts. In addition, the relevance of heat accumulation with multiple scanning passes and processing with multiple laser spots is shown.

***Corresponding author: Johannes Finger,** Chair for Laser Technology, RWTH Aachen University, Steinbachstr. 15, 52074 Aachen, Germany; and Fraunhofer Institute for Laser Technology, Steinbachstr. 15, 52074 Aachen, Germany, e-mail: finger@ilt.fraunhofer.de
Benedikt Bornschlegel: Chair for Laser Technology, RWTH Aachen University, Steinbachstr. 15, 52074 Aachen, Germany
Martin Reininghaus, Andreas Dohrn and Markus Nießen: Fraunhofer Institute for Laser Technology, Steinbachstr. 15, 52074 Aachen, Germany
Arnold Gillner and Reinhart Poprawe: Chair for Laser Technology, RWTH Aachen University, Steinbachstr. 15, 52074 Aachen, Germany; and Fraunhofer Institute for Laser Technology, Steinbachstr. 15, 52074 Aachen, Germany

www.degruyter.com/aot

Keywords: burst; heat accumulation; materials processing; ultrafast; USP.

1 Introduction

The application of ultrashort pulsed (USP) laser radiation with pulse durations in the range of several picoseconds down to some hundred femtoseconds enables materials processing with high resolution and precision in the micrometer range. Due to pulse durations, which are in the range of electron-phonon relaxation times for metallic materials, heat diffusion can be neglected and can result in quasi melt-free processing with negligible thermal load [1–4]. The extremely high precision, the advantage of a non-contact and wear-free tool, and the possibility to process nearly any material turn USP laser radiation into a versatile tool with emerging fields of application [5–7]. A continuously increasing field of application is the surface structuring of mold and embossing tools. While the processing quality meets the high demands of many applications, USP processing is currently lacking in terms of productivity, which still inhibits its economic application in many industrially relevant cases. Thus, upscaling of USP laser-based processes applying already available higher average power laser systems [8–13] to improve productivity and throughput is one major research topic in the field of process development for USP lasers.

The average power of a pulsed laser source is the product of pulse energy and repetition rate. Hence, there are two principal approaches for upscaling USP processes:

1. Scaling by increasing the pulse energy.
2. Scaling by increasing the pulse repetition rate.

As shown by Raciukaitis et al. [14] and Neuenschwander et al. [15], the appropriate fluence (pulse energy per focus area) is limited to some J/cm^2, due to efficiency and quality reasons. Due to this limitation, an upscaling using the first approach – by increasing the pulse energy – can be realized by splitting the pulse energy of the incoming

laser beam into multiple partial beams and realize parallel processing with an array of multiple laser foci. The beam splitting or separation is usually executed by applying diffractive optical elements (DOE) [16–18] or spatial light modulators [19, 20].

For the second approach, upscaling by increasing the repetition rate, fast beam deflection systems are necessary to control thermal and shielding effects. For fast beam deflection, an established approach is the use of polygon scanners [21–24] or fast rotating workpieces like printing or embossing cylinders to spatially separate subsequent pulses [25–27].

However, for both approaches, so-called heat accumulation is a central aspect that has to be taken into account. In this context, heat accumulation means the successive rise of the workpiece temperature by subsequent laser pulses with insufficient temporal and spatial separation [28]. Moreover, for USP laser processing, a distinct amount of the absorbed pulse energy does not contribute to the ablation process and remains as residual heat in the processed workpiece. For low average powers, this heat is negligible and dissipates into the bulk material. In contrast, for higher average power, this residual heat becomes relevant and has a significant influence on the processing results in terms of productivity and – more important – quality [29–32].

The term heat accumulation can be further differentiated into the following aspects:

1. Heat accumulation caused by subsequent pulses: The process that is usually meant by heat accumulation is the heat accumulation between subsequent laser pulses. When applying repetition rates in the range of some hundred kilohertz up to tens of megahertz, the time difference between subsequent pulses is too short to allow sufficient cooling of the workpiece between single laser pulses. In dependence on the repetition rate and spatial pulse distance, which determines how many pulses effectively contribute to heat accumulation of a certain volume of the workpiece, thermal effects occur that affect both ablation rate and achieved surface quality.
2. Heat accumulation caused by subsequent scanning passes: Additionally, heat accumulation on longer time scales can be relevant. As a consequence of the frequent repetition of scanning patterns with neighboring or overlapping processing tracks, thermal effects might occur even when one single isolated processing track has no significant influence. The relevance of heat accumulation between subsequent processing tracks is determined by time between the tracks, thermal input of one track, the number of tracks, and material properties.
3. Heat accumulation caused by multiple spots: When using multiple laser spots to realize power scaling via increased pulse energy, additional thermal effects have to be taken into account. Besides the heat input of every single beam, the thermal interaction or crosstalk between neighboring beams and the heat input across the whole beam pattern affects the local temperature of the workpiece. Here, the heat accumulation depends on workpiece factors like processed material and sample geometry, as well as the spatial distance between adjacent laser foci, the total number of applied spots, process parameters of every single beam, and the processing strategy.

The residual heat of one single ultrashort laser pulse, which accumulates and leads to relevant thermal input, is of fundamental value for understanding, describing, and controlling all of these thermal effects.

In the following sections, the effects of heat accumulation for USP processing with high average power will be discussed by giving an overview of the state of the art and original works as well. Thereby, theoretical approaches and experimental results will be presented to demonstrate USP processing with high repetition rates, pulse bursts, and multiple beams. Examples for beneficial and disadvantageous effects of heat accumulation are given.

First, a theoretical approach for describing the residual heat of a single ultrashort laser pulse is presented. After that, the aforementioned three types of heat accumulation will be discussed. For heat accumulation between subsequent tracks and during multi-beam processing, only an overview will be given, while thermal input of a single pulse and heat accumulation between subsequent pulses will be addressed more in detail.

2 Residual heat of a single ultrashort laser pulse

2.1 Theoretical description

The time scale that is relevant for heat accumulation processes depends on the thermal properties of the processed material, and is in the range of some nanoseconds up to some microseconds. This equals the typical temporal pulse-to-pulse distances during USP materials processing. Thus, imbalance of electron and phonon temperatures can be neglected and the classical heat conduction theory can be applied. As the heat input takes place on the time

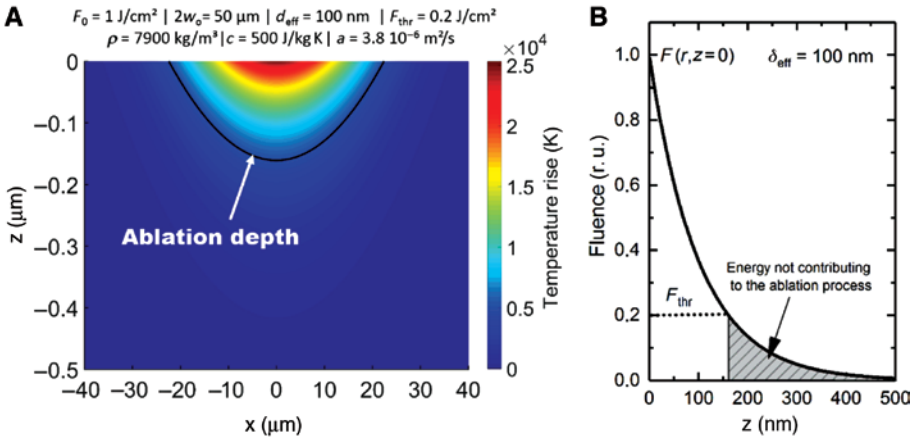

Figure 1: (A) Temperature distribution after absorption of a single ultrashort laser pulse. A distinct amount of the absorbed energy does not contribute to the ablation process and remains as residual heat in the processed workpiece. (B) Dependence of the fluence along the *z*-axis during the absorption process according to the Lambert-Beer law. The effective energy penetration depth is chosen to be 100 nm in this case. Due to the exponential decrease, a distinct amount of the absorbed energy remains in the workpiece, because the effective fluence is below the ablation threshold.

scale of the pulse duration, it is approximated as instantaneous [28].

Based on this assumption, an exemplary temperature distribution directly after absorption of a single ultrashort laser pulse with a Gaussian intensity distribution is shown in Figure 1A. In the presented case, the absorbed energy is higher than the material-specific ablation threshold. The ablated material leads to a parabolic ablation crater, as indicated with the black line.

As a consequence of the Gaussian intensity distribution and energy absorption according to the Lambert-Beer law, a distinct amount of the energy is absorbed in the surrounding area of ablation volume and will lead to heating of the workpiece, as shown in Figure 1B. For the relationships in Figure 1, an effective penetration depth of 100 nm has been chosen to clearly indicate the different energy amounts. The shown temperature distribution is directly after absorption, neglecting the imbalance of the electron and phonon system as described by the two-temperature model. Thus, the indicated temperatures are not physically reliable. However, the figure intends to show the different areas above and below the ablation threshold.

The energy of this effective heat source, E_{HA}, is described and related to the overall pulse energy, E_p:

$$\eta_{HA} = \frac{E_{HA}}{E_p}. \quad (1)$$

This ratio can be estimated on the basis of the following considerations: for those locations of the workpiece surface where the absorbed fluence is below the ablation threshold, all the pulse energy is converted into heat. That is the case for the side arms of the Gaussian intensity distribution. For locations of the surface at which the absorbed fluence is above the ablation threshold, the material is ablated. In the latter case, the heat input always equals the ablation threshold, because material is always ablated so deep until the effective fluence drops to the ablation threshold. Thus, in this case, an energy corresponding to the ablation threshold remains in the workpiece as residual heat.

For exemplary values of the fluence and ablation threshold, these are shown in Figure 2. The integral over the energy remaining in the workpiece and contributing to the heat input in relation to the overall pulse energy E_p gives a theoretical assumption for the factor η_{HA}:

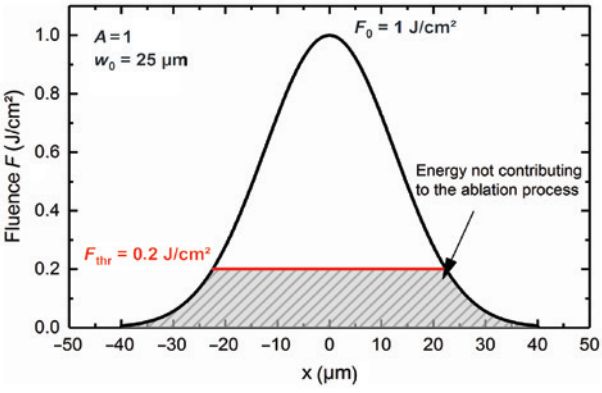

Figure 2: Spatial fluence distribution at the workpiece surface. The edges of the Gaussian distribution and the fraction of fluence below the ablation threshold form the effective heat source for a single ultrashort laser pulse.

$$\eta_{HA} = \frac{E_{HA}}{E_p} = \frac{A}{E_p} \cdot \left(\pi \cdot r_a^2 \cdot F_{\text{thr}} + \int_{r_a}^{\infty} F(r) \mathrm{d}r \mathrm{d}\varphi \right). \quad (2)$$

Here, r_a is the radius of the ablation crater, A the absorptivity of the workpiece surface, F_{thr} the ablation threshold, and $F(r)$ the radial fluence distribution.

Considering all dependencies, η_{HA} only depends on the ratio of F and F_{thr} and the absorptivity A.

In Figure 3, η_{HA} as a function of the ratio F/F_{thr} and for a typical absorptivity of a metallic material of 0.46 is shown.

For typically applied fluences, a factor of 8 above the ablation threshold, this simple theoretical approach predicts η_{HA} to be in the range of 0.2. However, the relationship shown is based on the assumption that there is no interaction of hot, ablated material with the workpiece. The evaporated material could transfer energy to the workpiece and thus leads to an additional heat source, increasing the effective amount of residual heat. However, interactions with particles or plasma can have the opposite effect by shielding the workpiece even before the energy is absorbed. Both of these effects result in derivations from the presented expectation.

Applying the approach of the superposition of instantaneous point sources [33], the temperature rise at a certain location x, y, z at time t, resulting from deposition of energy by a single laser pulse at $x = \Delta x$, $y = 0$, and $z = 0$, is described by

$$\Delta T_{SP}(t, x, y, z, \Delta x) = \int_{-\infty}^{\infty} \eta_{HA} \frac{F_0}{\rho c \delta_{\text{eff}}} \cdot e^{-2\left(\frac{(x'-\Delta x)^2 + y'^2}{w_0^2}\right)} \cdot e^{-\frac{z'}{\delta}} \cdot \frac{1}{\sqrt{4\pi a t}^3} e^{-\left[\frac{(\vec{x}-\vec{x}')^2}{4at}\right]} d\vec{x}', \; t > 0. \quad (3)$$

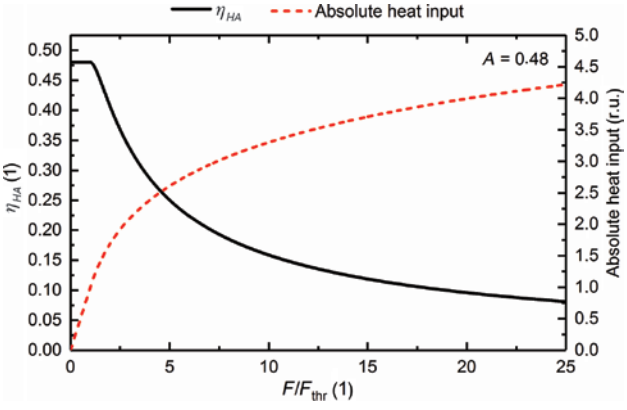

Figure 3: The factor η_{HA} (black) as a function of the ratio of applied fluence F and the ablation threshold F_{thr}. While the amount of residual heat decreases with increasing fluence, the overall heat input (red, dotted line) steadily increases with increasing fluence.

Here, ρ is the density of the processed material, c the heat capacity, w_0 the focus radius, a the thermal diffusivity, and δ_{eff} the effective energy penetration depth according to the Lambert-Beer law. In contrast to the expectation shown in Figure 2, the lateral shape of the effective heat source has been assumed to be Gaussian for this formula. Experimental measurement of the spatial geometry of the effective heat source, carried out by Bauer [34], show that this is an appropriate assumption.

2.2 Experimental determination

The value η_{HA} has been experimentally determined by Vorobyev et al. [35, 36] and by Bauer et al. [37] using a direct measurement based on a calorimetric setup. The determined values are in the range between 35% and 50% depending on the processed material. Vorobyev et al. reported that the residual energy increases to up to >70% with increasing applied fluence for ablation under ambient conditions. However, for ablation in vacuum, the amount of residual energy decreases with increasing fluence, as assumed on the basis of the presented theoretical estimation. Thus, indirect heat transfer from induced plasma to the workpiece may play a major role for applying high fluences.

A semi-empirical determination of the residual heat can be found in the study by Weber et al. [28]. They compared the experimental results of materials processing of carbon fiber-reinforced polymer (CFRP) and steel with theoretical predictions, and found good accordance of measurement and theory for $\eta_{HA} = 12.5\%$.

Another approach for an indirect determination of the residual heat is shown in Figures 4 and 5 for Inconel 718 as material. In a distinct parameter range, layers of molten material are induced at the sample surface (see also Section 3.2). The thickness of this layer can be determined with cross sections of the processed samples. The molten layer can be identified as a white layer in optical microscopy or based on the grain boundaries by laser scanning microscopy or scanning electron microscopy, as shown in Figure 4. In Figure 5, the measured maximum melting depth as a function of the applied repetition rate is shown for a constant fluence and feed per pulse. By comparing the experimentally obtained melting depth with theoretically predicted values (see also Section 3.1), a rough estimation of the amount of residual heat can be made. Assuming $\eta_{HA} = 0.25$, the theoretically predicted melting depth is in the same range as the measured one, as indicated in Figure 5. The melting depth can only be measured for high repetition rates and pulse overlaps. For such

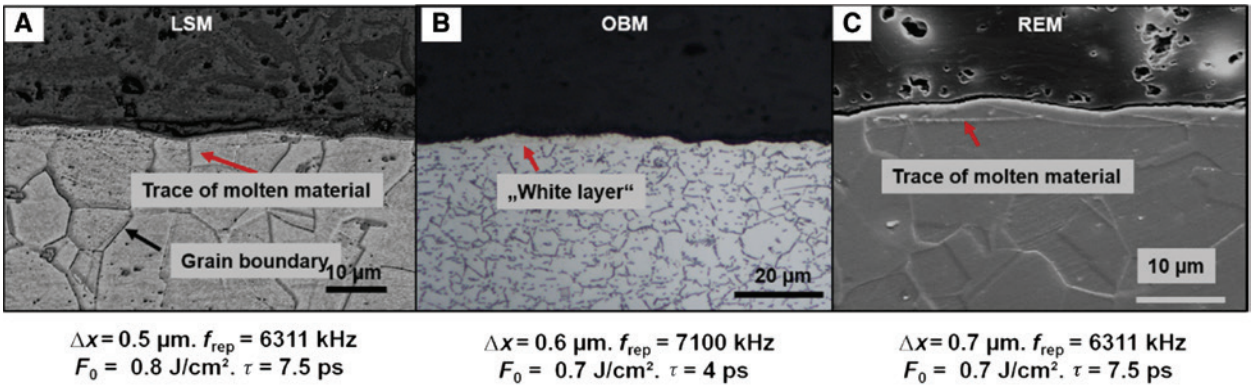

Figure 4: Cross sections of melting layers (material: Inconel 718). (A) Laser scanning microscopy, (B) optical bright-field microscopy, (C) scanning electron microscopy.

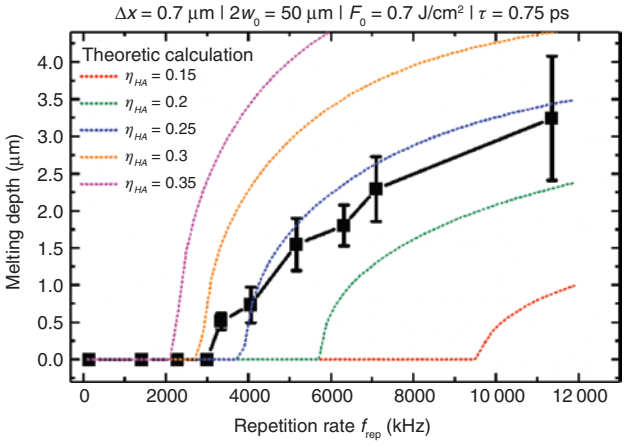

Figure 5: Experimentally determined melting depth as a function of repetition rate for constant feed per pulse, fluence, and pulse duration. The dotted lines represent the theoretically calculated melting depth for different values of η_{HA}. For choosing $\eta_{HA} = 0.25$, experiment and theory are at least in qualitatively good agreement (material: Inconel 718).

parameters, strong pulse-to-pulse interactions occur that lead to shielding and affect the factor η_{HA}. In comparison to results from other studies, the observed deviation might be connected to and explained by the shielding effects for processing with high repetition rates [31, 38, 39].

3 Heat accumulation caused by subsequent pulses

3.1 Theoretical description

To extend the theoretical description of the temperature rise after one single pulse to the temperature rise after N laser pulses with repetition rate f_{rep} and feed per pulse Δx, the superposition of all incident laser pulses has to be composed by building the sum over all subsequent pulses:

$$\Delta T_{MP}(t, \vec{x}, \Delta x, f_{rep}, N) = \sum_{i=1}^{N} \Delta T_{SP}(t - i \cdot f_{rep}, \vec{x}, i \cdot \Delta x) \cdot \Theta(t - i \cdot f_{rep}). \quad (4)$$

The resulting temperature rise for percussion drilling on a stainless-steel surface in dependence on the applied repetition rate is shown in Figure 6. With higher repetition rates, the cooling time between subsequent pulses is too short to enable a complete cool down of the sample surface. As a consequence, the workpiece temperature increases rapidly with high repetition rates. Moderate heat accumulation up to a distinct degree is not relevant for the process, as it does not affect processing quality or productivity. However, a pronounced heat accumulation affects the obtained surface quality significantly, as discussed in the following section.

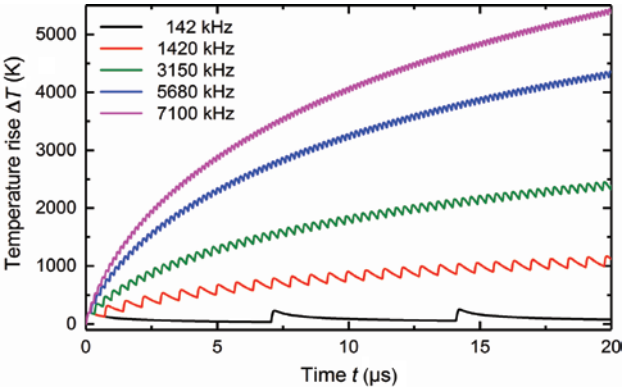

Figure 6: Theoretical temperature rise at the surface of a stainless-steel (V2A) sample for different repetition rates. The absorbed fluence is 0.1 J/cm² and there is no feed between subsequent pulses. Due to shorter cooling times, the temperature increases with increasing repetition rate (density $\rho = 7900$ kg/m³; heat capacity $c = 500$ J/kg K; temperature diffusivity $a = 3.8 \times 10^{-6}$ m²/s).

3.2 Influence on processing quality

Controlling heat accumulation is of paramount importance for scaling the productivity of USP processing. Even if heat accumulation does not lead to melting of the workpiece surface, the temperature rise due to accumulated heat affects the achievable surface quality. As shown by Bauer et al. [37], the generation of very rough, bumpy surface structures can be associated with heat accumulation. These surface structures – also called 'cone-like protrusions' – are a limit for the tolerable temperature rise during USP processing.

By varying processing parameters and the workpiece temperature using external pre-heating, Bauer et al. [37] identified that these rough structures emerge at a distinct surface temperature. In case of the examined stainless steel (V2A), that temperature is around 600°C.

For the processing of thermally sensitive materials like CFRP, an even smaller temperature rise caused by heat accumulation leads to comparable large heat-affected zones and is relevant as important mechanical properties are negatively affected by damaged matrix material [28].

The obtained surface morphologies for USP processing of Inconel 718 for different combinations of repetition rates and feed per pulse at constant fluences and pulse durations are shown in Figure 7. The different combinations of feed per pulse and repetition rate lead to an increasing effect of heat accumulation. Assuming a residual heat amount of 0.25, the energy per unit distance ranges from 0.3 J/m for the repetition rate of 140 kHz up to 5.6 J/m for the repetition rate of 14 200 kHz. In Figure 7A, the surface shows no significant effect of heat accumulation, while the surface in Figure 7B shows a very rough surface covered with cone-like protrusions. For even higher heat input, the surface starts to melt. This homogenous molten layer results in a very low surface roughness, as shown in Figure 7C. Therefore, heat accumulation can be beneficial for the process, as for high average power and ablation rates the observed homogenous melting layer in combination with the intrinsic surface tension of the molten phase enables a smoothing of the surface, resulting in a good surface quality, as demonstrated in Ref. [39]. A more pronounced heat accumulation leads to a re-increase of surface roughness due to inhomogeneous melt ejections, as shown in Figure 7D.

However, using fast beam deflection like a polygon scanner, USP processing at high repetition rates and average power without any significant effect of heat accumulation is possible. At high scanning speeds of several 100 m/s, the feed per pulse is sufficiently high to prevent heat accumulation from affecting the obtained surface quality. As shown in Figure 8, smooth, bump-free, and melt-free surfaces are generated with sufficiently high spatial pulse separation even with applying nearly 19 MHz and >200 W of average power.

3.3 Heat accumulation during burst processing

A special case of heat accumulation caused by subsequent laser pulses occurs during USP processing with pulse bursts. For USP processing with pulse bursts, a bunch of several pulses with a high repetition rate ($f_{burst} \approx 40–80$ MHz) is used instead of single laser pulses. Although the achieved ablation efficiency is reduced by pulse-to-pulse interactions [40], higher productivity can be achieved by applying pulse bursts, as much higher

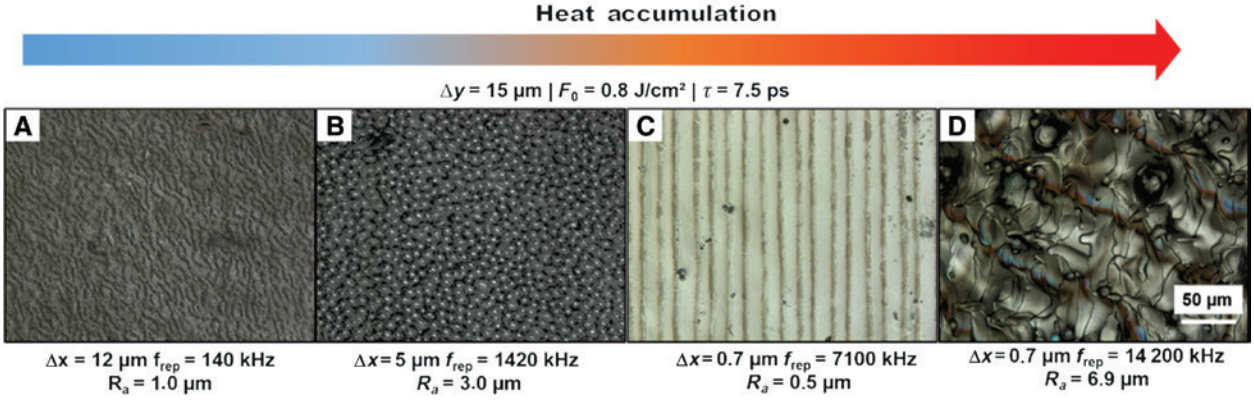

Figure 7: Development of obtained surface morphology with increasing amount of heat accumulation. (A) No influence of heat accumulation. (B) Generation of bump-like structures. (C) Homogenous melting layer induced by heat accumulation. (D) Rough surface due to melt ejection.

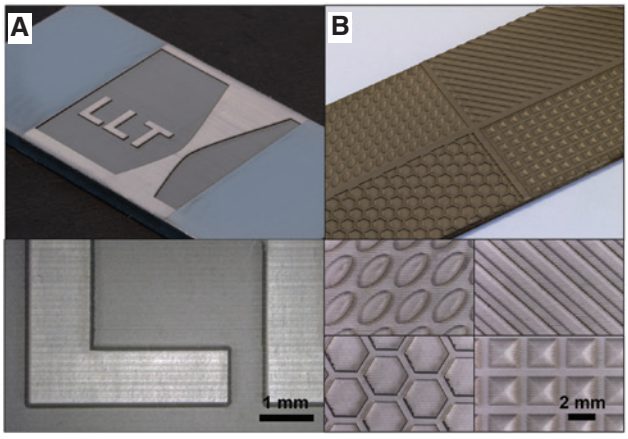

Figure 8: Results of USP processing of Inconel 718 with high repetition rate and average power. By using a polygon scanner for fast beam deflection, relevant affection of the surface quality by heat accumulation can be avoided. The average surface roughness is $R_a < 2$ µm. (A) Ablation rate 18.5 mm³/min using $P = 140$ W, $f_{rep} = 14\,400$ kHz, $\Delta x = 21$ µm, $2w_0 = 50$ µm. (B) Ablation rate 32 mm³/min using $P = 210$ W, $f_{rep} = 18\,900$ kHz, $\Delta x = 20$ µm, $2w_0 = 50$ µm.

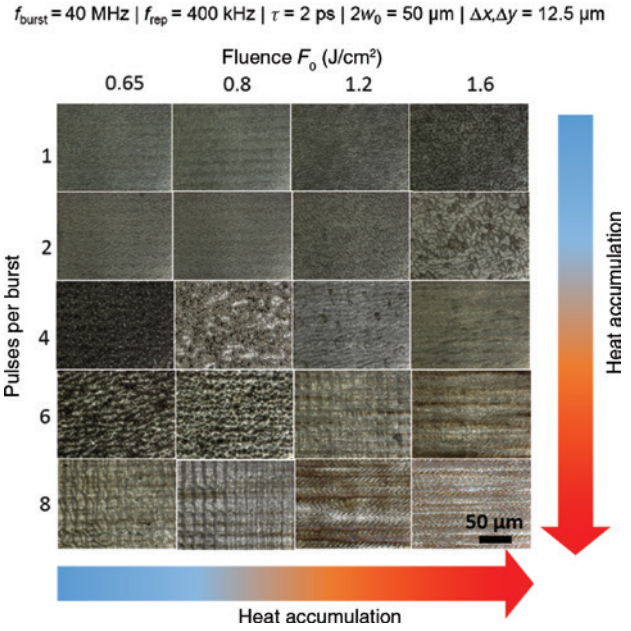

Figure 9: Obtained surface morphologies for USP burst processing of stainless steel for a varying numbers of pulses per burst and different single pulse fluences. The number of pulses per burst and the applied fluence determine the heat input and therefore lead to various effects of heat accumulation.

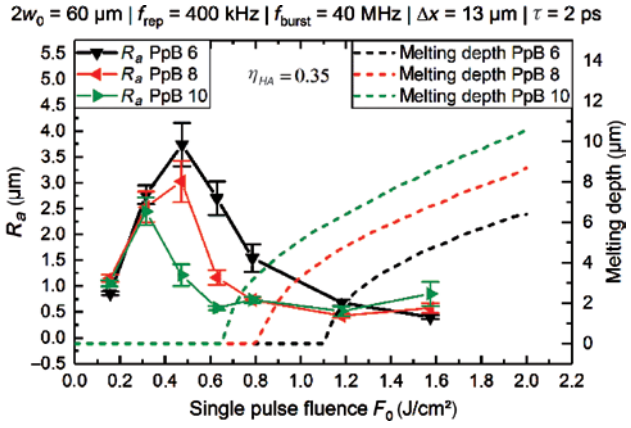

Figure 10: Average surface roughness for USP processing of stainless steel as a function of single pulse fluences. The theoretically obtained melting layers are indicated as dotted lines. The observed decrease of the surface roughness can qualitatively be associated with the occurrence of surface melting that helps smoothen the processed surface similar to a polishing process.

average powers can be applied even with conventional galvanometer scanners before the obtained surface roughness decreases. The use of pulse bursts aims for a targeted use and exploitation of heat accumulation to avoid rough surface structures while applying high average powers for USP processing. In Figure 9, the effect of the numbers of pulses within one burst and the applied fluence of a single pulse within the corresponding burst is illustrated. The amount of heat accumulation can be controlled by the number of pulses in one burst on the one hand side and the single pulse fluence on the other hand side. Thereby, the formation of surface morphologies is in agreement with the results presented in Section 3.2. For a distinct amount of heat accumulation, rough surface structures are induced (e.g. four pulses per burst, 0.65 J/cm²). The right amount of heat input avoids the formation of rough surface structures and enables the generation of smooth surfaces with high quality (e.g. four pulses per burst, 1.6 J/cm²). For even higher fluences or an increased number of pulses per burst, the increased heat accumulation leads to surfaces with noticeable thermal affection in terms of tarnishing.

For quantification, the measured R_a value as a function of applied fluence is shown in Figure 10 for different numbers of pulses within one burst. Starting with initially good R_a values around 1 µm, the surface roughness increases with increasing fluence and then drops again for a distinct fluence. The fluence at which the drop occurs depends on the applied number of pulses. Additionally, the theoretically expected melting depth is shown for a residual energy of 35% per pulse. The decrease of the obtained surface roughness is in qualitatively good agreement with the onset of surface melting.

An example for surface structuring of steel using pulse bursts is shown in Figure 11. The obtained surface is homogenous and free of bumps and pits. By using

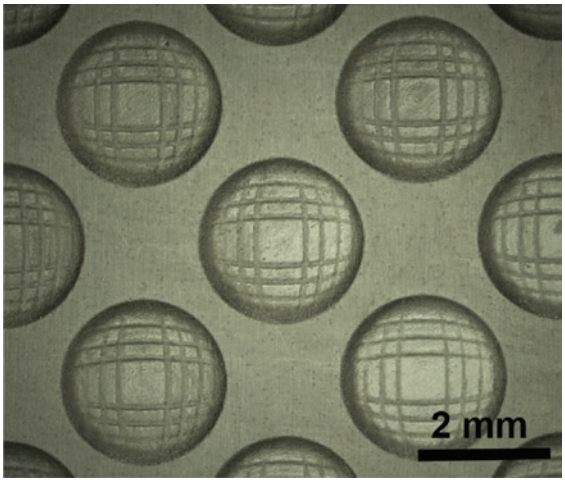

Figure 11: Surface structures (depth 200 µm) on stainless steel fabricated by means of picosecond pulse bursts. Using five pulses within one burst and an average power of 45 W, an ablation rate of 5.5 mm³/min can be realized ($2w_0 = 50$ µm, $f_{rep} = 400$ kHz, $f_{burst} = 40$ MHz, $\tau = 2$ ps, $F_0 = 2.2$ J/cm²).

the beneficial effect of heat accumulation, an average power of 45 W can be used to achieve an ablation rate of 5.5 mm³/min. However, the achieved ablation efficiency is 0.12 mm³/min W in this case. Compared to processing with single pulses and the same pulse duration, the efficiency is reduced by roughly 40%. At the same time, more than 8 times the average power can be applied, which overcompensates the loss of efficiency.

4 Heat accumulation caused by subsequent passes

The role of heat accumulation caused by subsequent passes of a scanning process has been investigated for cutting of CFRP with continuous wave laser radiation [41] as well as USP laser radiation [42, 43]. A systematic variation of time between subsequent passes and number of passes demonstrates the role of heat accumulation caused by subsequent passes onto the heat-affected zone for CFRP processing with picosecond laser pulses by Kononenko et al. [42]. An investigation of the effect for processing of thin metal sheets with picosecond pulses was done by Weber et al. [44]. The principle behavior and effects of heat accumulation caused by subsequent passes are similar to the heat accumulation caused by subsequent pulses but on a completely different time scale. While the effect of heat accumulation caused by subsequent passes has an obvious impact on the processing of thermally sensitive materials like CFRP, the impact of this effect during processing of metals is much less pronounced, but plays an important role for the reproducibility of especially small surface structures. Thus, processing results do not only depend on direct processing parameters, like repetition rate, power, focus diameter, and hatch distance, but also on scanning strategies and structure sizes.

In Figure 12, equal, hemispheric surface structures are shown, which were fabricated with the same processing parameters but different scanning strategies. For the structure shown in (A), a field of structures was fabricated by generating every structure one after another. For the structure shown in (B), the array of structures was processed layer by layer, across the whole pattern, resulting in an increased time between subsequent layers of one structure. The structures of both scan strategies look very similar and exhibit good quality in terms of geometry and surface roughness. However, the structures that were processed structure after structure are slightly deeper than the structures processed via layer-by-layer strategy. The average depth of the structures processed one after another was 36.6 ± 0.5 µm, while the structures processed layer by layer reached an average depth of 30.8 ± 0.3 µm only. This result can be attributed to the heat accumulation between adjacent scanning passes and subsequent layers, increasing the achieved ablation rate by the preheating effect due to the different cooling times for applying the two different scan strategies. For fabricating such small structures in the range of 100 µm one structure after another, subsequent passes and layers follow with almost no cooling time. The structures were generated using pulse bursts, which further increased the relevance of accumulation caused by subsequent scans.

5 Heat accumulation during multi-beam processing

For materials processing with USP laser radiation with high pulse energy, multi-beam processing is an effective approach to homogeneously distribute the pulse energy across the surface of the workpiece without losing the high resolution of materials processing by means of USP laser radiation with a small focal size. Here, every single laser process is tuned to the working point of highest efficiency and multiplied by the number of beams. In this manner, the throughput for the generation of accurate periodic structures can be significantly increased. Moreover, with the use of multiple laser spots, high average laser power can be applied even for repetition rates that

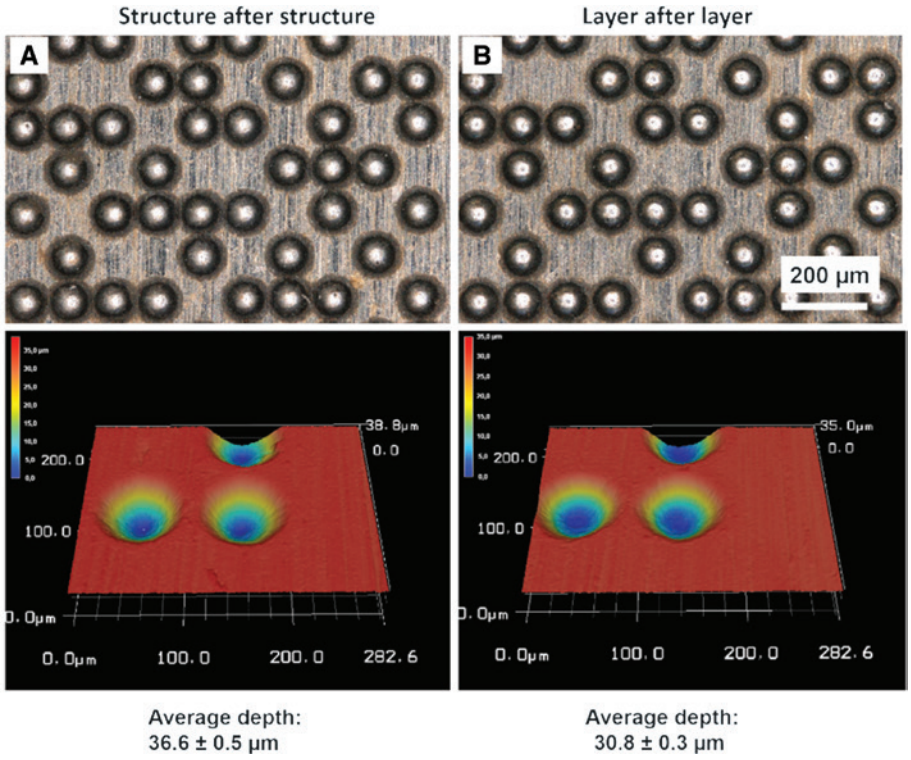

Figure 12: Surface structures on stainless steel fabricated with USP laser radiation using pulse bursts. The shown arrays of hemispherical surface structures are processed with the same laser processing parameters but different scan strategies. The structures shown in (A) are processed one after another, while the structures shown in (B) are processed layer by layer, meaning that one layer of the whole pattern of structures is processed before the next layer is started. The structures for both processing strategies appear very similar in geometries and quality, but the structures processed one after the other show an increased depth of nearly 20%. Due to the reduced cooling time of the structure after structure scan strategy (A), heat accumulation caused by subsequent passes and layers becomes relevant and increases the ablation depth as a result of pre-heating of the workpiece.

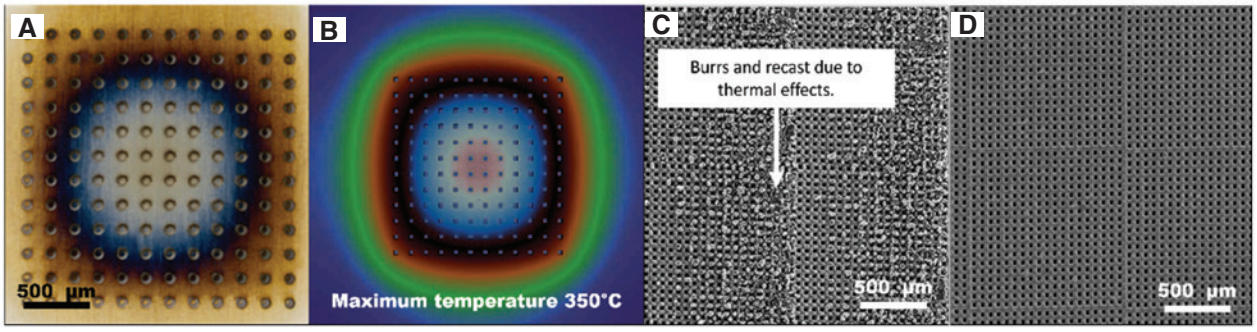

Figure 13: (A) Annealing colors of a parallelized 12×12 multi-beam drilling process of stainless steel. (B) Temperature distribution calculated by a multi-scale simulation approach. (C) Burr and recast increase as thermal interaction between adjacent beams increases during the meander-like scan strategy on 30-µm-thin stainless steel. (D) Same structure and identical process time as shown in (C), but with an optimized thermal management by means of an adapted process parameters and scan strategy.

are small enough to limit the negative effects of heat accumulation.

However, in addition to the aforementioned effects, the heat input of the multi-beam pattern during materials processing leads to an additional temperature rise that can affect the processing results.

In Figure 13A, the result of percussion drilling of a thin steel foil with a 12 times 12 beam array, generated by a static DOE, is shown. The interaction between the heat sources within the spot array causes location-dependent, macroscopic thermal input that causes the generation of annealing colors in the shown case. For

smaller structures, such thermal spot-to-spot interaction leads to burrs and recast when processing thermally sensitive materials, as shown in Figure 13C. A simulation of the shown process as illustrated in Figure 13B is in need of a multi-scale approach as presented by Nießen et al. [45]. The complete steps from heat input of a single laser pulse to the heat during drilling a hole and up to the thermal interaction between the different spots within one array have to be taken into account. For a homogenous processing result (Figure 13D), the heat accumulation of a multi-laser foci pattern needs to be controlled by processing strategies and the distance of the laser beams. However, one of the most important factors to avoid strong heat accumulation is the choice of efficient processing parameters for each single beam to limit the heat input right from the start.

6 Conclusions and outlook

This paper gives an overview of the thermal effects during USP processing, covering heat input, heat accumulation, and concrete impacts on processing results. In addition to the description of the state of the art, some new and original works are presented.

Controlling of heat input is one major challenge in the upscaling of USP processes to higher average power. The fundamental basis to understand and control thermal effects is to understand the heat input resulting from one single pulse. The amount of the incident pulse energy that remains as residual heat in the workpiece was measured to be in the range of 30%–40%. Indirect measurements by comparing theoretical predictions and experimental results determine the factor in the range of 12.5%. On this topic, we present as a new approach to determine this factor the comparison of theoretically and experimentally simulated melt depths. The residual heat determined by this indirect approach is in the range of 25%. A detailed understanding of the heat input of a single pulse and the dependency on processing parameters like fluence and pulse duration is an open task. Besides the classical heat accumulation caused by subsequent pulses, heat accumulation caused by subsequent scanning passes also has to be taken into account for the processing of thermally sensitive materials or small structure sizes. We present the influence of these effects for the fabrication of small structures on steel. By influencing the thermal input, the chosen scan strategy significantly affects the achieved structure geometry and has to be taken into account for the precise, deterministic fabrication of these structures.

For USP processing with multiple laser spots, heat input plays an important role. In addition to heat accumulation between pulses and passes, the interaction between the different laser foci is a relevant factor that has to be taken into account for an optimized thermal management during multi-beam processing.

However, controlling heat input and accumulation enables the use of high average powers to achieve high productivity and excellent processing qualities. Heat accumulation is not always obstructive and can also help increase productivity and surface quality when it is controlled and handled in the right way. Compared to processing using longer pulsed laser sources like nanosecond lasers, USP processing with exactly controlled heat input (like processing with bursts) enables a much better processing quality in terms of precision and avoidance of burrs or thermal affection to the workpiece structure.

Acknowledgments: Parts of this work have been funded by the German Research Foundation DFG under grant no. PO 591/41-1.

References

[1] B. N. Chichkov, C. Momma, S. Nolte, F. Alvensleben and A. Tünnermann, Appl. Phys. A, 63, 109–115 (1996).
[2] S. Nolte, C. Momma, H. Jacobs, A. Tünnermann, B. N. Chichkov, et al., J. Opt. Soc. Am. B 14, 2716–2722 (1997).
[3] S.-S Wellershoff, J. Hohlfeld, J. Güdde and E. Matthias, Appl. Phys. A 69, S99–S107 (1999).
[4] K.-H. Leitz, B. Redlingshöfer, Y. Reg, A. Otto and M. Schmidt, Phys. Proc. 12, 230–238 (2011).
[5] B. Jaeggi, B. Neuenschwander, M. Schmid, M. Muralt, J. Zuercher, et al., Phys. Proc. 12, 164–171 (2011).
[6] S. L. Campanelli, A. D. Ludovico, C. Bonserio, P. Cavalluzzi and M. Cinquepalmi, J. Mater. Process. Technol. 191, 220–223 (2007).
[7] M. Henry, P. M. Harrison, I. Henderson and M. F. Brownell, Proc. SPIE 5662 (2004). Doi: 10.1117/12.596743.
[8] T. Eidam, D. Schimpf, O. Schmidt, B. Ortaç, K. Rademaker, et al., Opt. Lett. 35, 94 (2010).
[9] P. Russbüldt, T. Mans, G. Rotarius, J. Weitenberg, H. D. Hoffmann, et al., Opt. Lett. 17, 12230–12245 (2009).
[10] P. Russbüldt, T. Mans, J. Weitenberg, H. D. Hoffmann and R. Poprawe, Opt. Lett. 35, 4169–4171 (2010).
[11] J.-P. Negel, A. Voss, M. A. Ahmed, D. Bauer, D. Sutter, et al., Opt. Lett. 38, 5442 (2013).
[12] P. Russbueldt, D. Hoffmann, M. Höfer, J. Löhring, J. Luttmann, et al., IEEE J. Select. Top. Quant. Electron. 21, 447–463 (2015).
[13] J. Limpert, T. Schreiber, T. Clausnitzer, K. Zöllner, H.-J. Fuchs, et al., Opt. Express 10, 628 (2002).

[14] G. Raciukaitis, M. Brikas and M. Gedvilas, in 'Proceedings of ICALEO 2008' (2008), p. M403.
[15] B. Neuenschwander, B. Jaeggi, V. Romano and S. M. Pimenov, in 'Laser Applications in Microelectronic and Optoelectronic Manufacturing (LAMOM) XVII' (2012).
[16] O. Haupt, V. Schütz and U. Stute, in 'Laser-based Micro- and Nanopackaging and Assembly V' (2011).
[17] L. Büsing, S. Eifel and P. Loosen, in 'SPIE Photonics Europe 2014, Proceedings Volume 9131, Optical Modelling and Design III', vol. 9131 (Brussels, Belgium, 2014), pp. 91310C-91310C-12.
[18] J.-I. Kato, N. Takeyasu, Y. Adachi, H.-B. Sun and S. Kawata, Appl. Phys. Lett. 86, 044102 (2005).
[19] Z. Kuang, D. Liu, W. Perrie, S. Edwardson, M. Sharp, et al., Appl. Surf. Sci. 255, 6582–6588 (2009).
[20] Z. Kuang, W. Perrie, D. Liu, S. Edwardson, J. Cheng, et al., Appl. Surf. Sci. 255, 9040–9044 (2009).
[21] R. De Loor, Phys. Proc. 41, 544–551 (2013).
[22] J. Schille, L. Schneider and U. Loeschner, Appl. Phys. A 120, 847–855 (2015).
[23] B. Jaeggi, V. Romano and S. M. Pimenov, in 'Laser Applications in Microelectronic and Optoelectronic Manufacturing (LAMOM) XIX' (2014).
[24] U. Loeschner, J. Schille, A. Streek, T. Knebel and L. Hartwig, J. Laser Appl. 27, S29303 (2015).
[25] G. Hennig, S. Bruening and B. Neuenschwander, in 'CLEO:2011 – Laser Applications to Photonic Applications' (2011).
[26] G. Hennig, K.-H. Selbmann and A. Brockelt, in 'Workshop on Laser Applications in Europe' (2005).
[27] S. Bruening, G. Hennig, S. Eifel and A. Gillner, Phys. Proc. 12, 105–115 (2011).
[28] R. Weber, T. Graf, P. Berger, V. Onuseit, M. Wiedenmann, et al., Opt. Express 22, 11312 (2014).
[29] A. Ancona, F. Röser, K. Rademaker, J. Limpert, S. Nolte, et al., Opt. Express 16, 8958 (2008).
[30] A. Ancona, S. Döring, C. Jauregui, F. Röser, J. Limpert, et al., Opt. Lett. 34, 3304 (2009).
[31] J. Finger and M. Reininghaus, Opt. Express 22, 18790–18799 (2014).
[32] F. Di Niso, C. Gaudiuso, T. Sibillano, F. P. Mezzapesa, A. Ancona, et al., Opt. Express 22, 12200 (2014).
[33] H. S. Carslaw and J. C. Jaeger, 'Conduction of Heat in Solids' (Clarendon Pr., Oxford, 1959).
[34] F. Bauer, J. Laser Micro/Nanoeng. 10, 325–328, 2015.
[35] A. Y. Vorobyev, V. M. Kuzmichev, N. G. Kokody, P. Kohns, J. Dai, et al., Appl. Phys. A 82, 357362 (2005).
[36] A. Y. Vorobyev and C. Guo, Appl. Phys. Lett. 86, 011916 (2005).
[37] F. Bauer, A. Michalowski, T. Kiedrowski and S. Nolte, Opt. Express 23, 1035 (2015).
[38] J. König, S. Nolte and A. Tünnermann, Opt. Express 13, 10597 (2005).
[39] J. Finger, C. Kalupka and M. Reininghaus, J. Mater. Process. Technol. 226, 221227 (2015).
[40] B. Neuenschwander, Th. Kramer, B. Lauer and B. Jaeggi, in 'Laser Applications in Microelectronic and Optoelectronic Manufacturing (LAMOM) XX' (2015).
[41] D. Herzog, M. Schmidt-Lehr, M. Canisius, M. Oberlander, J.-P. Tasche, et al., J. Laser Appl. 27, S28001 (2015).
[42] T. V. Kononenko, C. Freitag, M. S. Komlenok, V. Onuseit, R. Weber, et al., J. Appl. Phys. 118, 103105 (2015).
[43] C. Freitag, M. Wiedenmann, J.-P. Negel, A. Loescher, V. Onuseit, et al., Appl. Phys. A 119, 1237–1243 (2015).
[44] R. Weber, T. Graf, C. Freitag, A. Feuer, T. Kononenko, et al., Opt. Express 25, 3966–3979 (2017).
[45] M. Nießen, L. Bürgermeister and N. Hambach, Laser Technik J. 14, 42–44 (2017).